# Accurate double many-body expansion potential energy surface of $HS_2(A\,^2A')$ by scaling the external correlation*

Lu-Lu Zhang(张路路), Yu-Zhi Song(宋玉志)†, Shou-Bao Gao(高守宝), Yuan Zhang(张媛), and Qing-Tian Meng(孟庆田)‡

*School of Physics and Electronics, Shandong Normal University, Jinan* 250014, *China*

(Received 22 December 2015; revised manuscript received 25 January 2016; published online 1 April 2016)

A globally accurate single-sheeted double many-body expansion potential energy surface is reported for the first excited state of $HS_2$ by fitting the accurate *ab initio* energies, which are calculated at the multireference configuration interaction level with the aug-cc-pV*QZ* basis set. By using the double many-body expansion-scaled external correlation method, such calculated *ab initio* energies are then slightly corrected by scaling their dynamical correlation. A grid of 2767 *ab initio* energies is used in the least-square fitting procedure with the total root-mean square deviation being 1.406 kcal·mol$^{-1}$. The topographical features of the $HS_2(A\,^2A')$ global potential energy surface are examined in detail. The attributes of the stationary points are presented and compared with the corresponding *ab initio* results as well as experimental and other theoretical data, showing good agreement. The resulting potential energy surface of $HS_2(A\,^2A')$ can be used as a building block for constructing the global potential energy surfaces of larger S/H molecular systems and recommended for dynamic studies on the title molecular system.

**Keywords:** potential energy surface, *ab initio* calculation, $HS_2$, transition state

**PACS:** 31.15.A–, 31.15.ae, 31.50.Bc **DOI:** 10.1088/1674-1056/25/5/053101

## 1. Introduction

Sulfur-containing species have received growing attention due to their important role played in the air pollution and acid rain.[1–7] Among various sulfur-containing compounds, the $HS_2$ radical is one of the most important species, which is responsible for the oxidation of reduced forms of sulfur, the reaction in combustion[8–10] and biochemistry.[11,12] Therefore, extensive studies on the $HS_2$ radical have been carried out both theoretically and experimentally for decades.

Among a vast array of theoretical studies, Sannigrahi *et al.*[13] performed CI calculations and provided both structural and vibrational information of the electronic ground and excited states of $HS_2$. Zhou *et al.*[14] carried out investigations on the geometries and spectroscopic parameters of the $XS_2$ ($X$ = H, F, Al, and Br) radicals using the split-valence plus polarization function and larger basis sets at the self-consistent field (SCF) and the second order Møller–Plesset (UMP2). By employing the CCSD(T) theory, the equilibrium structure and vibrational frequencies were reported by Owens *et al.*[15] for the $X_2H$ hydrides ($X$ = Al, Si, P, and S) at their global minima. Subsequently, more accurate structural and thermodynamic properties of the $HS_2$ radical were obtained by Denis[16] using the CCSD(T) and B3LYP levels of theory. Later, the accurate three-dimensional, near-equilibrium potential energy and dipole moment functions for both the ground and the first electronic excited states of $HS_2$ were constructed by Peterson *et al.*[17] by using highly correlated coupled cluster methods with explicit basis set extrapolation. Song *et al.*[18] reported an accurate double many-body expansion (DMBE) potential energy surface (PES) for ground-state $HS_2$ based on *ab initio* energies extrapolated to the complete basis set limit. Quite recently, Qin *et al.*[7] calculated the equilibrium geometry of the first excited electronic state of $HS_2$ by time-dependent density functional theory using the hybrid functional B3LYP with the aug-cc-pV*QZ* (AV*QZ*) basis set.

The vibrational frequencies of the ground state ($X^2A''$) and the excited state ($A^2A'$) of $HS_2$ were investigated by Holstein *et al.*[19] By studying the microwave spectroscopy of the ground electronic state of $HS_2$, Yamanoto and Saito[20] reported the lowest energy structure. Ashworth *et al.*[21] first observed the far infrared laser magnetic resonance (LMR) spectrum of the ground state of $HS_2$. Subsequently, Isoniemi *et al.*[22] investigated more refined structural information of $HS_2$ radical in Ar matrix following the 266 nm photolysis of $H_2S_2$. The S–H stretching and the S–S–H bending modes were observed at 2463 cm$^{-1}$ and 903 cm$^{-1}$, respectively. Ashworth and Fink[23] analyzed the $X$–$A$ band system through high-resolution Fourier-transform measurements of the chemiluminescence spectra of both $HS_2$ and $DS_2$. Entfellner and

*Project supported by the National Natural Science Foundation of China (Grant No. 11304185), the Taishan Scholar Project of Shandong Province, China, the Shandong Provincial Natural Science Foundation, China (Grant No. ZR2014AM022), the Shandong Province Higher Educational Science and Technology Program, China (Grant No. J15LJ03), the China Postdoctoral Science Foundation (Grant No. 2014M561957), and the Post-doctoral Innovation Project of Shandong Province, China (Grant No. 201402013).

†Corresponding author. E-mail: yzsong@sdnu.edu.cn

‡Corresponding author. E-mail: qtmeng@sdnu.edu.cn

© 2016 Chinese Physical Society and IOP Publishing Ltd 

Boesl[24] presented the photodetachment-photoelectron spectra of the ground and the first excited states of $HS_2$ and $DS_2$ with a conventional time of flight photoelectron spectrometry.

Indeed, as far as we are aware, there is no work toward obtaining a global PES for the first electronic excited state of $HS_2(A^2A')$ reported, which would be of interest to the investigations of the $H(^2S) + S_2(a^1\Delta_g) \rightarrow SH(X^2\Pi) + S(^3P)$ reaction. Thus, the major goal of the present work is to obtain a high quality global PES of $HS_2(A^2A')$ based on the DMBE[25–28] methodology.

This paper is organized as follows. Section 2 describes the *ab initio* calculations employed in the present work. Section 3 presents a brief description of the analytical DMBE formalism. Then the major topographical features of the $HS_2(A^2A')$ PES are discussed in Section 4. The concluding remarks are summarized in Section 5.

## 2. *Ab initio* calculations

The *ab initio* calculations have been carried out at the multi-reference configuration interaction level[29,30] of theory, including the Davidson correction [MRCI(Q)],[31] using the full valence complete-active-space self-consistent field (CASSCF)[32] wave function as the reference. The AV*QZ* basis set of Dunning[33,34] is employed, and the *ab initio* calculations are performed using the Molpro 2012 package.[35] A grid of 2767 *ab initio* points is chosen to map the PES over the H–$S_2$ region defined by $2.5 \leq R_{S_2}/a_0 \leq 5.5$, $0.2 \leq r_{H-S_2}/a_0 \leq 15$, $0^\circ \leq \gamma/ \leq 90^\circ$, and for the S–SH interactions, $2.0 \leq R_{SH}/a_0 \leq 4.0$, $0.6 \leq r_{S-SH}/a_0 \leq 15$, $0^\circ \leq \gamma/ \leq 180^\circ$, where $R$, $r$, and $\gamma$ are the atom–diatom Jacobi coordinates. The $C_s$ point group symmetry is employed in the *ab initio* calculations, which holds two irreducible representations A′ and A″. For $HS_2(A^2A')$, seven A′ and two A″ symmetry molecular orbitals (MOs) are determined as the active space, amounting to 214 (136A′ + 78A″) configuration state functions. The MOs which correlate with the 3s and 3p atomic orbitals of each S and the 1s orbital of the H atom are utilized to determine the valence space.

The *ab initio* energies calculated in this way have been subsequently corrected using the double many-body expansion-scaled external correlation method (DMBE-SEC)[36] to account for the excitations beyond singles and doubles, most importantly, for incompleteness of the basis set. According to the DMBE-SEC scheme, the total DMBE-SEC interaction energy is written as

$$V(\boldsymbol{R}) = V_{\rm FVCAS}(\boldsymbol{R}) + V_{\rm SEC}(\boldsymbol{R}), \tag{1}$$

where

$$V_{\rm FVCAS}(\boldsymbol{R}) = \sum_i V^{(2)}_{i,\rm FVCAS}(R_i) + V^{(3)}_{\rm FVCAS}(\boldsymbol{R}), \tag{2}$$

$$V_{\rm SEC}(\boldsymbol{R}) = \sum_i V^{(2)}_{i,\rm SEC}(R_i) + V^{(3)}_{\rm SEC}(\boldsymbol{R}). \tag{3}$$

The first terms of Eqs. (2) and (3) sum over all the diatomic components with $i = AB, BC, AC$, and $\boldsymbol{R} = \{R_{AB}, R_{AC}, R_{BC}\}$ in $V^{(3)}_{\rm FVCAS}(\boldsymbol{R})$ and $V^{(3)}_{\rm SEC}(\boldsymbol{R})$ is a collective variable of all internuclear distances. Then $V^{(2)}_{i,\rm SEC}(R_i)$ and $V^{(3)}_{\rm SEC}(\boldsymbol{R})$ in Eq. (3) are expressed as

$$V^{(2)}_{i,\rm SEC}(R_i) = \frac{V^{(2)}_{i,\rm MRCI}(R_i) - V^{(2)}_{i,\rm FVCAS}(R_i)}{F^{(2)}_i}, \tag{4}$$

$$V^{(3)}_{\rm SEC}(\boldsymbol{R}) = \frac{V^{(3)}_{\rm MRCI}(\boldsymbol{R}) - V^{(3)}_{\rm FVCAS}(\boldsymbol{R})}{F^{(3)}}. \tag{5}$$

Following the previous work,[37–39] the scaling factors $F^{(2)}_i$ in Eq. (4) are chosen to reproduce the corresponding bond dissociation energies of the $i$-th diatom, while $F^{(3)}$ in Eq. (5) is estimated as the average of the three two-body $F$-factors. The scaling factors obtained with the AV*QZ* basis set are $F^{(2)}_{\rm SS}$=0.7331, $F^{(2)}_{\rm SH}$=0.8536, and $F^{(3)}$=0.8134.

## 3. Analytic form of DMBE potential energy surface

In the framework of DMBE methodology, the single-sheeted PES can be written as

$$V(\boldsymbol{R}) = \sum_i^3 [V^{(2)}_{\rm EHF}(R_i) + V^{(2)}_{\rm dc}(R_i)] + V^{(3)}_{\rm EHF}(\boldsymbol{R}) + V^{(3)}_{\rm dc}(\boldsymbol{R}), \tag{6}$$

where $\boldsymbol{R} = (R_1, R_2, R_3)$ is a collective diatomic internuclear separation, and the two-body and the three-body energy terms are split into two contributions: the extended Hartree–Fock (EHF) and the dynamical correlation (dc) energies. The following subsections give a detailed description of the two-body and the three-body energy terms in Eq. (6).

### 3.1. Two-body energy terms

The diatomic potential energy curves (PECs) of $S_2(a^1\Delta_g)$ and $SH(X^2\Pi)$, which show the correct behaviors at the asymptotic limits $R \rightarrow 0$ and $R \rightarrow \infty$, have been modeled using the EHF approximate correlation energy method.[40,41]

The EHF-type energy term is written as

$$V^{(2)}_{\rm EHF}(R) = -D/R(1 + \sum_{i=1}^{7} a_i r^i)\exp(-\gamma r), \tag{7}$$

where

$$\gamma = \gamma_0[1 + \gamma_1 \tan(\gamma_2 r)]. \tag{8}$$

Here $r = R - R_e$ is the displacement from the equilibrium diatomic geometry; $D$, $a_i$ $(i = 1, \ldots, 7)$, and $\gamma_i$ $(i = 0, 1, 2)$ are adjustable parameters to be obtained from a least-square fitting procedure.

In turn, the dc energy term is written as[42]

$$V^{(2)}_{\rm dc}(R) = -\sum_{n=6,8,10} C_n \chi_n(R) R^{-n}, \tag{9}$$

with the damping functions for the dispersion coefficients assuming the form

$$\chi_n(R) = [1 - \exp(-A_n R/\rho - B_n R^2/\rho^2)]^n, \quad (10)$$

where $A_n = \alpha_0 n^{-\alpha_1}$ and $B_n = \beta_0 \exp(-\beta_1 n)$ are auxiliary functions. The $\alpha_0, \beta_0, \alpha_1$, and $\beta_1$ are universal dimensionless parameters for all isotropic interactions: $\alpha_0 = 16.36606$, $\alpha_1 = 0.70172$, $\beta_0 = 17.19388$, and $\beta_1 = 0.09574$. Moreover, $\rho/a_0 = 5.5 + 1.25R_0$, where $R_0 = 2(\langle r_A^2\rangle^{1/2} + \langle r_B^2\rangle^{1/2})$ is the LeRoy parameter,[43] and $\langle r_A^2\rangle$ and $\langle r_B^2\rangle$ are the expectation values of the squared radii for the outermost electrons in atoms $A$ and $B$, respectively.

### 3.2. Three-body energy terms

As usual,[44,45] the three-body dc energy term is written in the following functional form:

$$V_{\rm dc}^{(3)} = -\sum_i \sum_n f_i(\boldsymbol{R}) \chi_n(r_i) C_n^{(i)}(R_i, \theta_i) r_i^{-n}, \quad (11)$$

where $R_i$ is the corresponding diatomic internuclear separation, $r_i$ is the distance between atom $A$ and the center-of-mass of diatom $BC$, and $\theta_i$ is the angle between these two vectors. $f_i(\boldsymbol{R}) = \{1 - \tanh[\xi(\eta R_i - R_j - R_k)]\}/2$ is a switching function. As was done in Ref. [37], we have used $\eta = 6$ and $\xi = 1.0 a_0^{-1}$. The $\chi_n(r_i)$ in Eq. (11) is a damping function, which is written in the functional form employed elsewhere.[37,44] As was done for $NH_2(2\,^2A'')$,[46] the parameters of $V_{\rm dc}^{(3)}$ are taken from Ref. [18] for the ground electronic state of $HS_2$.

For a given triatomic geometry, by removing the sum of the two-body energy terms from the corresponding interaction energies, one obtains the total three-body energy. Then by subtracting the three-body dc contribution from the total three-body energy, the three-body EHF energy contribution is obtained. It can be modeled in the three-body distributed-polynomial[47] form

$$V_{\rm EHF}^{(3)} = \sum_{j=1}^{3} P^j(Q_1, Q_2, Q_3) \times \prod_{I=1}^{3} \{1 - \tanh[\gamma_i^j (R_i - R_i^{j,\rm ref})]\}, \quad (12)$$

where $P^j(Q_1, Q_2, Q_3)$ is the $j$-th polynomial up to six-order in symmetry coordinates, which is defined as

$$\begin{aligned} &P^j(Q_1, Q_2, Q_3) \\ &= C_1^j + C_2^j Q_1 + C_3^j Q_3 + C_4^j Q_1^2 + C_5^j S_{2a}^2 + C_6^j Q_1 Q_3 \\ &+ C_7^j S_{2b}^2 + C_8 Q_1^3 + C_9^j Q_1 S_{2a}^2 + C_{10}^j S_3^3 + C_{11}^j Q_1^2 Q_3 + C_{12}^j Q_1 S_{2b}^2 \\ &+ C_{13}^j Q_3 S_3^3 + C_{14}^j Q_1^4 + C_{15}^j Q_1^2 S_{2a}^2 + C_{16}^j S_{2a}^4 + C_{17}^j Q_1 S_3^3 \\ &+ C_{18}^j Q_1^3 Q_3 + C_{19}^j Q_1^2 S_{2b}^2 + C_{20}^j Q_1 Q_3 S_{2a}^2 \\ &+ C_{21}^j Q_3 S_3^2 + C_{22}^j S_{2a}^2 S_{2b}^2 + C_{23}^j Q_1^5 + C_{24}^j Q_1^3 S_{2a}^2 \\ &+ C_{25}^j Q_1 S_{2a}^4 + C_{26}^j Q_1^2 S_3^3 + C_{27}^j S_{2a}^2 S_3^3 \\ &+ C_{28}^j Q_1^4 Q_3 + C_{29}^j Q_1^3 S_{2b}^2 + C_{30}^j Q_1^2 Q_3 S_{2a}^2 + C_{31}^j Q_1 Q_3 S_3^3 \\ &+ C_{32}^j Q_1 S_{2a}^2 S_{2b}^2 + C_{33}^j Q_3 S_{2a}^4 + C_{34}^j S_{2b}^2 S_3^3 + C_{35}^j Q_1^6 + C_{36}^j Q_1^4 S_{2a}^2 \\ &+ C_{37}^j Q_1^2 S_{2a}^4 + C_{38}^j Q_1^3 S_3^3 + C_{39}^j Q_1 S_{2a}^2 S_3^3 + C_{40}^j S_{2a}^6 + + C_{41}^j S_3^6 \\ &+ C_{42}^j Q_1^5 Q_3 + C_{43}^j Q_1^4 S_{2b}^2 + C_{44}^j Q_1^3 Q_3 S_{2a}^2 \\ &+ C_{45}^j Q_1^2 Q_3 S_3^3 + C_{46}^j Q_1^2 S_{2a}^2 S_{2b}^2 + C_{47}^j Q_1 Q_3 S_{2a}^4 \\ &+ C_{48}^j Q_1 S_{2b}^2 S_3^3 + C_{49}^j Q_3 S_{2a}^2 S_3^3 + C_{50}^j S_{2a}^4 S_{2b}^2. \end{aligned} \quad (13)$$

In the above equation, $S_{2a}^2 = Q_2^2 + Q_3^2$, $S_{2b}^2 = Q_2^2 - Q_3^2$, and $S_3^2 = Q_3^3 - 3Q_2^2 Q_3$, with $Q_i$ $(i = 1, 2, 3)$ being the symmetry coordinates defined as

$$\begin{bmatrix} Q_1 \\ Q_2 \\ Q_3 \end{bmatrix} = \begin{bmatrix} \sqrt{(1/3)} & \sqrt{(1/3)} & \sqrt{(1/3)} \\ \sqrt{(1/2)} & -\sqrt{(1/2)} & 0 \\ -\sqrt{(1/6)} & -\sqrt{(1/6)} & \sqrt{(2/3)} \end{bmatrix} \begin{bmatrix} R_1 - R_1^{j,\rm ref} \\ R_2 - R_2^{j,\rm ref} \\ R_3 - R_3^{j,\rm ref} \end{bmatrix}. \quad (14)$$

In turn, $R_i^{j,\rm ref}$ are the reference geometries and $\gamma_i^j$ are the nonlinear range-determining parameters, which are optimized via a trial-and-error least-squares fitting procedure[48,49] that minimizes the root-mean-squared deviation (rmsd) error while warranting the proper behavior in the asymptotic region. The complete set of parameters totals 150 linear coefficients, 9 nonlinear ones, and 9 reference geometries. Table 1 shows the rmsd values of the final DMBE/SEC PES with respect to all the fitted *ab initio* energies. As shown in Table 1, a total of 2676 points have been used for the calibration procedure, thus covering a range up to 400 kcal·mol$^{-1}$ above the $HS_2$ global minimum.

**Table 1.** Root-mean-square deviations (in kcal·mol$^{-1}$) of the PES.

| Energy/kcal·mol$^{-1}$ | $N^{\rm a}$ | rmsd | $N^{\rm b}_{>\rm rmsd}$ |
|---|---|---|---|
| 10 | 24 | 0.206 | 12 |
| 20 | 65 | 0.491 | 14 |
| 30 | 133 | 0.925 | 34 |
| 40 | 217 | 1.046 | 54 |
| 50 | 321 | 1.103 | 91 |
| 60 | 769 | 1.221 | 148 |
| 70 | 1157 | 1.279 | 193 |
| 80 | 1286 | 1.321 | 224 |
| 90 | 1703 | 1.276 | 307 |
| 100 | 1807 | 1.289 | 333 |
| 200 | 2520 | 1.341 | 443 |
| 300 | 2631 | 1.371 | 463 |
| 400 | 2676 | 1.406 | 461 |

[a] Number of points in the indicated energy range.

[b] Number of points with an energy deviation larger than the rmsd.

## 4. Features of potential energy surface

The fitted potential energy curves of $S_2(a\,^1\Delta_g)$ and $SH(X\,^2\Pi)$ and the deviations from the MRCI(Q)/AV$QZ$ energies are displayed in Fig. 1. As shown in Fig. 1, the modeled PECs show smooth behaviors and accurately mimic the *ab initio* energies, with the maximum error being smaller than 0.05 kcal·mol$^{-1}$. Parameters gathered in Table 2 include

the equilibrium geometry ($R_e$), dissociation energy ($D_e$), harmonic vibrational frequency ($\omega_e$), non-harmonic vibrational frequency ($\omega_e x_e$), and rotational constants ($\alpha_e$ and $\beta_e$). Excellent agreement can be found in Table 2 between the results obtained from the modeled PECs and the experimental data. For $SH(X^2\Pi)$, the deviations for $R_e$, $D_e$, $\omega_e$, $\omega_e x_e$, $\alpha_e$, and $\beta_e$ are calculated to be $0.0002a_0$, $0.3948 kcal \cdot mol^{-1}$, $5.736\ cm^{-1}$, $0.447\ cm^{-1}$, $0.0346\ cm^{-1}$, and $0.1304\ cm^{-1}$, respectively, while the corresponding deviations for $S_2(a^1\Delta_g)$ are $0.0199a_0$, $0.15\ cm^{-1}$, $0.845\ cm^{-1}$, $0.00017\ cm^{-1}$, and $0.0033\ cm^{-1}$. Good agreement is also found compared to other theoretical results.[17,18,50–53]

Figures 2–4 illustrate the major topographical features of the $HS_2(A^2A')$ DMBE/SEC PES, and the corresponding structural parameters of the stationary points are collected in Table 3, including our *ab initio* values calculated at the MRCI(*Q*)/AV*QZ* level of theory and other theoretical and experimental results. The global minimum obtained from the

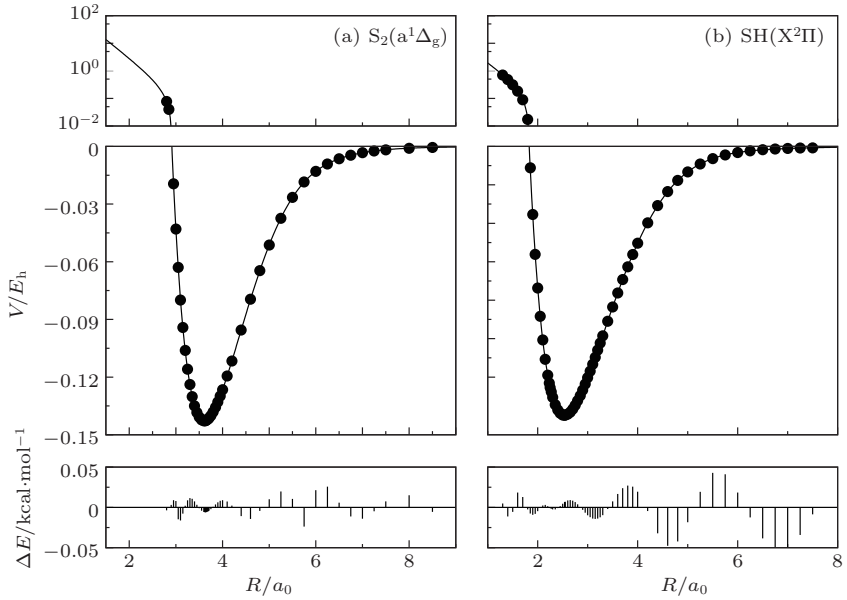



**Fig. 1.** Potential energy curves of (a) $S_2(a^1\Delta_g)$ and (b) $SH(X^2\Pi)$, and the differences between the fitted PECs and the *ab initio* points.

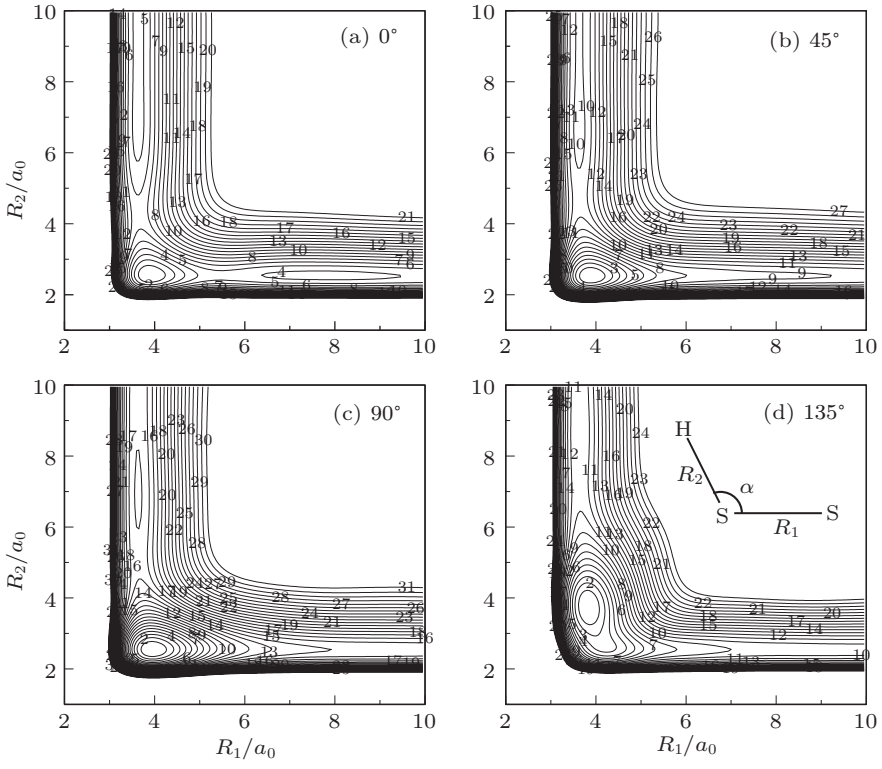



**Fig. 2.** Contour plots of $HS_2(A^2A')$ potential energies for the four H–S–S angles (a) 0°, (b) 45°, (c) 90°, and (d) 135°. Contours are equally spaced by $0.006E_h$, starting from $-0.1668E_h$ in panel (a), $-0.1977E_h$ inpanel (b), $-0.2294E_h$ in panel (c), and $-0.2006E_h$ in panel (d).

**Table 2.** Spectroscopic constants of SH and $S_2$ diatoms, $R_e$ is in the units of a.u., $D_e$ is in the units of kcal·mol$^{-1}$, and $\omega_e$, $\omega_e x_e$, $\alpha_e$, and $\beta_e$ are in the units of cm$^{-1}$.

| | $R_e$ | $D_e$ | $\omega_e$ | $\omega_e x_e$ | $\alpha_e$ | $\beta_e$ |
|---|---|---|---|---|---|---|
| | | | SH($X^2\Pi$) | | | |
| This work | 2.5337 | 87.7448 | 2701.536 | 59.453 | 0.3046 | 9.5965 |
| Theor.[18] | 2.5354[a] | 87.77[a] | 2697.5[a] | – | – | – |
| Theor.[17] | 2.5325[b] | 87.56[b] | 2701.2[b] | – | – | – |
| Theor.[58],[c] | 2.5376 | 87.13 | 2699.8 | 47.706 | 0.2639 | 9.4414 |
| Exp.[59,60] | 2.5339 | 87.35±0.7 | 2695.8 | 59.9 | 0.270 | 9.4611 |
| | | | $S_2(a^1\Delta_g)$ | | | |
| This work | 3.6079 | 89.5674 | 702.20 | 3.935 | 0.0019 | 0.2893 |
| Theor.[50] | 3.6007 | 89.5322 | 700.81 | 3.921 | 0.0019 | 0.2905 |
| Theor.[51] | 3.5972 | 89.0832 | 699.68 | 3.102 | 0.0017 | 0.2911 |
| Theor.[52] | 3.6050 | – | 746 | – | 0.0014 | 0.2897 |
| Theor.[53] | 3.6070 | – | 697.0 | – | – | – |
| Exp.[59] | 3.588 | – | 702.35 | 3.09 | 0.00173 | 0.2926 |

[a] Obtained from $HS_2(X^2A'')$ PES.
[b] The dissociation energies are calculated by $D_e = D_0 + \omega_e/2$.
[c] Obtained at CCSD(T)/AV5Z level of theory.

**Table 3.** Properties of stationary points on the fitted $HS_2(A^2A')$ PES (harmonic frequencies in cm$^{-1}$).

| Feature | $R_1/a_0$ | $R_2/a_0$ | $R_3/a_0$ | $E/E_h$ | $\omega_{H-S}$ | $\omega_{S-S}$ | $\omega_{bending}$ |
|---|---|---|---|---|---|---|---|
| | | | | Global minimum | | | |
| DMBE/SEC PES | 3.937 | 2.540 | 4.836 | –0.2298 | 2714.19 | 504.45 | 812.71 |
| MRCI($Q$)/AV$QZ$ | 3.962 | 2.538 | 4.833 | –0.2220 | 2640.73 | 425.84 | 862.64 |
| Theor.[17] | 3.923 | 2.536 | 4.790 | – | 2674.1 | 513.0 | 770.5 |
| Theor.[16] | 3.942 | 2.538 | 4.808 | – | 2683 | 501 | 765 |
| Theor.[15] | – | – | – | – | 2706 | 517 | 794 |
| Exp.[23] | – | – | – | – | | 504.5 | 808 ± 10 |
| Exp.[24] | – | – | – | – | 2550 ± 200 | 750 ± 200 | |
| Exp.[7] | – | – | – | – | 2585 ± 81 | 490 ± 41 | 741 ± 41 |
| | | | | TS1 ($C_{2v}$) | | | |
| DMBE/SEC PES | 3.987 | 2.965 | 2.965 | –0.1889 | 1406.44 | 481.93 | 1823.40i |
| MRCI($Q$)/AV$QZ$ | 3.933 | 2.928 | 2.928 | –0.2006 | 1932.39 | 541.41 | 1395.79i |
| | | | | TS2 ($C_{\infty v}$) | | | |
| DMBE/SEC PES | 3.891 | 6.445 | 2.555 | –0.1667 | 2446.84 | 478.52 | 712.60i |
| MRCI($Q$)/AV$QZ$ | 3.991 | 6.829 | 2.838 | –0.1476 | 1154.95 | 309.25 | 407.15i |
| | | | | SP1 ($D_{\infty v}$) | | | |
| DMBE/SEC PES | 5.870 | 2.935 | 2.935 | –0.1241 | 1756.21i | 385.43 | 225.78i |
| MRCI($Q$)/AV$QZ$ | 6.042 | 3.021 | 3.021 | –0.1153 | 2668.31i | 295.29 | 273.13i |
| | | | | SP2 ($C_{\infty v}$) | | | |
| DMBE/SEC PES | 3.652 | 4.265 | 7.917 | –0.1288 | 219.85i | 724.26i | 628.07 |
| | | | | SP3 ($C_{\infty v}$) | | | |
| DMBE/SEC PES | 5.457 | 2.537 | 7.994 | –0.1392 | 474.65i | 193.09i | 2656.44 |

present DMBE/SEC PES locates at $R_1 = 3.937a_0$, $R_2 = 2.540a_0$, and $R_3 = 4.836a_0$ ($R_1$ is the SS interatomic separation, while $R_2$ and $R_3$ are the two SH interatomic separations), differing only $0.025a_0$, $0.002a_0$, and $0.003a_0$ from the MRCI($Q$)/AV$QZ$ results, respectively. Compared with the theoretical works of Peterson *et al.*[17] and Denis,[16] the maximal differences occur in $R_3$, which are only $0.043a_0$ and $0.025a_0$, respectively. Since the DMBE-SEC method is employed to model the *ab initio* energies, the well depth of the global minimum is $0.0078E_h$ lower than that of MRCI($Q$)/AV$QZ$. As for the harmonic frequencies, the DMBE/SEC PES from the present work predicts values of 2714.19 cm$^{-1}$, 504.45 cm$^{-1}$, and 812.27 cm$^{-1}$, which are in good agreement with the most recent experimental values given by Qin *et al.*,[7] which are $2585 \pm 81$ cm$^{-1}$, $490 \pm 41$ cm$^{-1}$, and $741 \pm 41$ cm$^{-1}$, respectively. Table 3 also gathers the properties of three saddle points

(SP): SP1 ($D_{\infty v}$), SP2 ($C_{\infty v}$), and SP3 ($C_{\infty v}$), and two transition states (TS): TS1 ($C_{2v}$) and TS2 ($C_{\infty v}$).

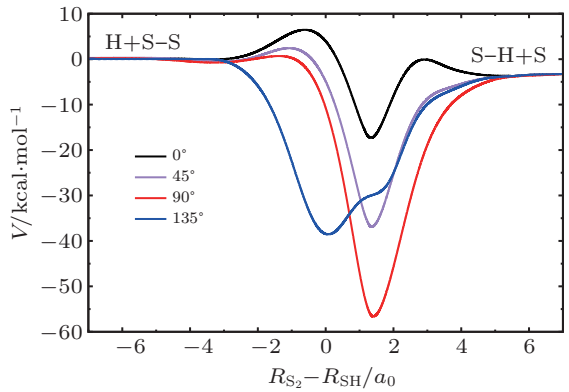



**Fig. 3.** (color online) Minimum energy paths for $HS_2(A^2A')$ PES at four H–S–S angles.

The contour maps for the $H(^2S) + S_2(a^1\Delta_g) \rightarrow SH(X^2\Pi) + S(^3P)$ reaction in internal coordinates at four H–S–S angles ($\angle HSS = 0°$, 45°, 90°, and 135°) are shown in Fig. 2. The contours are equally spaced by $0.006E_h$, starting at $-0.16681E_h$ for 0°, $-0.19773E_h$ for 45°, $-0.22936E_h$ for 90°, and $-0.20061E_h$ for 135°. The notable feature observed is that there are two valleys in each map: the left upper valley corresponds to $H(^2S) + S_2(a^1\Delta_g)$ asymptote, while the valley at the right bottom corresponds to $SH(X^2\Pi) + S(^3P)$ asymptote. It can also be seen in Fig. 2 that deep wells connect the two asymptotes. For a better understanding of the characteristics of the present PES, the minimum energy paths (MEPs) of the $H(^2S) + S_2(a^1\Delta_g) \rightarrow SH(X^2\Pi) + S(^3P)$ reaction at the four H–S–S angles are shown in Fig. 3. These MEPs represent the potential energies of $HS_2(A^2A')$ as a function of a suitable reaction coordinate defined as $R_{S_2} - R_{SH}$, where $R_{S_2}$ and $R_{SH}$ are the S–S and S–H internuclear distances, respectively. The $R_{S_2}$ approaches the $S_2$ equilibrium distance when the reaction coordinate is large, whereas a large positive reaction coordinate corresponds to $R_{SH}$ approaching the SH equilibrium distance. The exothermicity of the $H(^2S) + S_2(a^1\Delta_g) \rightarrow SH(X^2\Pi) + S(^3P)$ reaction is 3.6 kcal · mol$^{-1}$. The salient feature when $\angle HSS = 0°$, 45°, 90°, and 135° is that there exist the deep wells at 17.30 kcal · mol$^{-1}$, 36.85 kcal · mol$^{-1}$, 56.45 kcal · mol$^{-1}$, and 38.56 kcal · mol$^{-1}$ relative to the H + $S_2$ reactant, respectively. As shown in Fig. 3, there also exist barriers when $\angle HSS = 0°$, 45°, 90°, and the highest barrier (6.459 kcal · mol$^{-1}$ relative to H + $S_2$ reactant) is obtained when $\angle HSS = 0°$, locating at $R_{S_2} = 3.652a_0$ and $R_{SH} = 4.265a_0$.

Figure 4 shows the spherically averaged isotropic ($V_0$) and leading anisotropic potentials ($V_2$) for H + $S_2$ and S + SH scattering processes. The $V_L$ ($L = 0, 2$) potentials are obtained by expressing the interaction energies in a Legendre expansion[54–56]

$$V(R_e, r, \theta) = \sum_L V_L(R_e, r) P_L(\cos\theta), \tag{15}$$

where $R_e$ are the internuclear separations of $S_2$ and SH, which are fixed at their equilibrium values of $3.6079a_0$ and $2.5337a_0$, $r$ and $\theta$ are the Jacobi coordinates, and $P_L$ are the Legendre polynomials. Then, the $V_L$ potentials can be calculated by the following integral:[57]

$$V_L(R_e, r) = (2L+1) \times \int_0^{\pi/2} V(\boldsymbol{R}) P_L(\cos\theta) \sin\theta \, d\theta. \tag{16}$$

The isotropic average potential ($V_0$) determines how close on average the atom and the diatom can approach each other. In turn, the sign of $V_2$ indicates whether or not the molecule prefers to orient its axis along the direction of the incoming atom: a negative value favors the collinear approach, while a positive value favors the approach through an isosceles triangular geometry. As shown in Fig. 4(a), $V_2$ is positive at distances larger than $5.50a_0$ and smaller than $8.20a_0$, which indicates that the H atom favors approaching the $S_2$ diatom in this region through an isosceles triangular geometry. For the S + SH interaction displayed in Fig. (b), there is no barrier in $V_0$, while the $V_2$ component is non-negative in the regions of interest, which corroborate the fact that the interaction favors the insertion of the S atom perpendicularly to the SH diatom.

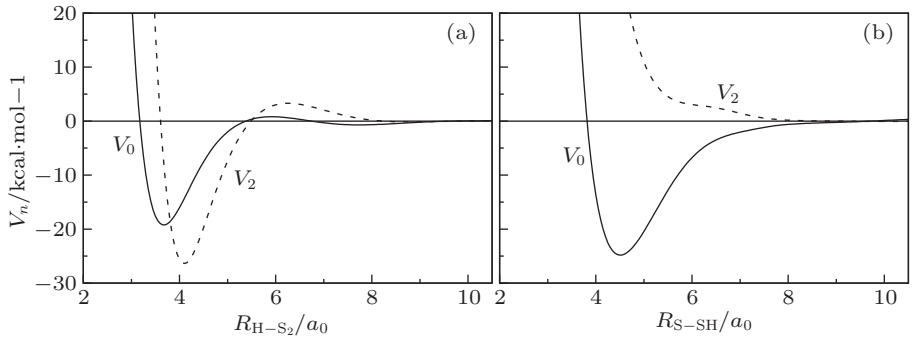



**Fig. 4.** The spherically averaged isotropic ($V_0$) and leading anisotropic potentials ($V_2$): (a) for H + $S_2$ interaction, with $R_{SS} = 3.6079a_0$; (b) for S + SH interaction, with $R_{SH} = 2.5337a_0$.

## 5. Conclusion

A global accurate PES is reported for $HS_2(A^2A')$ by fitting the MRCI($Q$)/AV$QZ$ energies which are scaled by the DMBE-SEC method. The resulting PES is realistic over the entire configuration space. The various topographical features of the current DMBE/SEC PES have been examined in detail and compared with the previous theoretical and experimental results. The properties, including geometries, energies, and vibrational frequencies, have been characterized on the current $HS_2(A^2A')$ DMEB-SEC PES. The results show good agreement with the previous high quality theoretical studies and the available experiment data. Thus, the PES constructed here can be used for dynamic studies of reactions and also as a building block for the PESs of larger molecular systems containing the $HS_2$ fragment.

## References


[1] Moran S and Ellison G B 1988 *J. Phys. Chem.* **92** 1794
[2] Friedl R R, Brune W H and Anderson J G 1985 *J. Phys. Chem.* **89** 5505
[3] Smardzewski R R and Lin M C 1977 *J. Chem. Phys.* **66** 3197
[4] Balucani N, Beneventi L, Casavecchia P, Stranges D and Volpi G. G 1991 *J. Chem. Phys.* **94** 8611
[5] Wang N S and Howard C J 1990 *J. Phys. Chem.* **94** 8787
[6] Lovejoy E R, Wang N S and Howard C J 1987 *J. Phys. Chem.* **91** 5749
[7] Qin Z, Cong R, Liu Z, Xie H and Tang Z 2014 *J. Chem. Phys.* **141** 204312
[8] Glavas S and Toby S 1975 *J. Phys. Chem.* **79** 779
[9] Sendt K, Jazbec M and Haynes B S 2002 *Proc. Combust. Inst.* **29** 2439
[10] Gargurevich I A 2005 *Ind. Eng. Chem. Res.* **44** 7706
[11] Whiteman M, Cheung N S, Zhu Y Z, Chu S H, Siau J L, Wong B S, Armstrong J S and Moore P K 2005 *Biochem. Biophys. Res.* **326** 794
[12] Huxtable R 1986 *Biochemistry of Sulphur* (New York: Plenum Press)
[13] Sannigrahi A B, Peyerimhoff S D and Buenker R J 1977 *Chem. Phys. Lett.* **46** 415
[14] Zhuo Q, Clouthier D J and Goddard J D 1994 *J. Chem. Phys.* **100** 2924
[15] Owens Z T, Larkin J D and Schaefer III H F 2006 *J. Chem. Phys.* **125** 164322
[16] Denis P A 2006 *Chem. Phys. Lett.* **422** 434
[17] Peterson K A, Mitrushchenkov A and Francisco J S 2008 *Chem. Phys.* **346** 34
[18] Song Y Z and Varandas A J C 2011 *J. Phys. Chem. A* **115** 5274
[19] Holstein K, Fink E, Wildt J and Zabel F 1985 *Chem. Phys. Lett.* **113** 1
[20] Yamamoto S and Saito S 1994 *Can. J. Phys.* **72** 954
[21] Ashworth S H, Evenson K M and Brown J M 1995 *J. Mol. Spectrosc.* **172** 282
[22] Isoniemi E, Khriachtchev L, Pettersson M and Räsänen M 1999 *Chem. Phys. Lett.* **311** 47
[23] Ashworth S H and Fink E H 2007 *Mol. Phys.* **105** 715
[24] Entfellner M and Boesl U 2009 *Phys. Chem. Chem. Phys.* **11** 2657
[25] Varandas A J C 2004 *Advanced Series in Physical Chemistry* (Sigapor: World Scientific Publishing) p. 91
[26] Varandas A J C, Brand ao J and Quintales A M 1988 *J. Phys. Chem.* **92** 3732
[27] Varandas A J C 2000 *Lecture Notes in Chemistry* (Laganá A and Riganelli A Eds.) (Berlin: Springer) Vol. **75** pp. 33–56
[28] Varandas A J C 1985 *J. Mol. Struct. Theochem.* **120** 401
[29] Werner H J and Knowles P J 1988 *J. Chem. Phys.* **89** 5803
[30] Werner H J and Knowles P J 1988 *Chem. Phys. Lett.* **145** 514
[31] Langhoff S R and Davidson E R 1974 *Int. J. Quantum Chem.* **8** 61
[32] Knowles P J and Werner H J 1985 *Chem. Phys. Lett.* **115** 259
[33] Dunning Jr T H 1989 *J. Chem. Phys.* **90** 1007
[34] Kendall R A, Dunning Jr T H and Harrison R J 1992 *J. Chem. Phys.* **96** 6796
[35] Werner H J, Knowles P J, Knizia G, Manby F R, Schütz M, *et al.* 2012 *Molpro* version 2012.1, a package of *ab initio* programs
[36] Varandas A J C 1992 *Chem. Phys. Lett.* **194** 333
[37] Varandas A J C and Poveda L A 2006 *Theor. Chem. Acc.* **116** 404
[38] Song Y Z, Li Y Q, Gao S B and Meng Q T 2014 *Eur. Phys. J. D* **68** 1
[39] Song Y Z, Zhang Y, Zhang L L, Gao S B and Meng Q T 2015 *Chin. Phys. B* **24** 63101
[40] Varandas A J C 1988 *Adv. Chem. Phys.* **74** 255
[41] Varandas A J C and Silva J D 1992 *J. Chem. Soc. Faraday Trans.* **88** 941
[42] Varandas A J C 1987 *Mol. Phys.* **60** 527
[43] Le Roy R J 1973 *Spec. Period. Rep. Chem. Soc. Mol. Spectrosc.* **1** 113
[44] Varandas A J C 1996 *J. Chem. Phys.* **105** 3524
[45] Li Y Q, Yuan J C, Chen M D, Ma F C and Sun M T 2013 *J. Comput. Chem.* **34** 1686
[46] Li Y Q. Ma F C and Sun M T 2013 *J. Chem. Phys.* **139** 154305
[47] Martínez-Núñez E and Varandas A J C 2001 *J. Phys. Chem. A* **105** 5923
[48] Li Y Q, Zhang P Y and Han K L 2015 *J. Chem. Phys.* **142** 124302
[49] Li Y Q, Song Y Z, Song P, Li Y Z, Ding Y, Sun M T and Ma F C 2012 *J. Chem. Phys.* **136** 194705
[50] Zhang L L, Gao S B, Meng Q T and Song Y Z 2015 *Chin. Phys. B* **24** 13101
[51] Xing W, Shi D, Sun J, Liu H and Zhu Z 2013 *Mol. Phys.* **111** 673
[52] Swope W C, Lee Y and Schaefer H F 1979 *J. Chem. Phys.* **70** 947
[53] Peterson K A, Lyons J R and Francisco J S 2006 *J. Chem. Phys.* **125** 084314
[54] Varandas A J C, Brown F B, Mead C A, Truhlar D G and Blais N C 1987 *J. Chem. Phys.* **86** 6258
[55] Varandas A J C 1987 *Chem. Phys. Lett.* **138** 455
[56] Varandas A J C and Tennyson J 1981 *Chem. Phys. Lett.* **77** 151
[57] Murrell J N, Carter S, Farantos S C, Huxley P and Varandas A J C 1984 *Molecular Potential Energy Functions* (Chicheste: Wiley)
[58] Shi D H, Zhang J P, Sun J F, Liu Y F, Zhu Z L, Ma H and Yang X D 2008 *Chin. Phys. B* **17** 3678
[59] Huber K P and Herzberg G 1979 *Molecular Spectra and Molecular Structure Constants of Diatomic Molecules* (New York: van Nostrand Reinhold)
[60] Continetti R E, Balko B A and Lee Y T 1991 *Chem. Phys. Lett.* **182** 400